Chemistry Faculty Research & Creative Works   Chemistry

01 Jan 2006

A Comparative Study of the Properties of Polar and Nonpolar Solvent/Solute/Polystyrene Solutions in Microwave Fields Via Molecular Dynamics

Mark J. Purdue

Macduff O. Okuom

Frank D. Blum
Missouri University of Science and Technology

James M. D. MacElroy

et. al. For a complete list of authors, see https://scholarsmine.mst.edu/chem_facwork/2351

Recommended Citation

M. J. Purdue et al., "A Comparative Study of the Properties of Polar and Nonpolar Solvent/Solute/Polystyrene Solutions in Microwave Fields Via Molecular Dynamics," *Journal of Chemical Physics*, American Institute of Physics (AIP), Jan 2006.
The definitive version is available at https://doi.org/10.1063/1.2353112

A comparative study of the properties of polar and nonpolar solvent/solute/polystyrene solutions in microwave fields via molecular dynamics

Mark J. Purdue, J. M. D. MacElroy,[a] and D. F. O'Shea
UCD School of Chemical and Bioprocess Engineering, University College Dublin, Belfield, Dublin 4, Ireland; The Centre for Synthesis and Chemical Biology, University College Dublin, Belfield, Dublin 4, Ireland; and Conway Institute of Biomolecular and Biomedical Research, University College Dublin, Belfield, Dublin 4, Ireland

Macduff O. Okuom and Frank D. Blum
Department of Chemistry, University of Missouri-Rolla, Rolla, Missouri 65401-0010 and Graduate Center for Materials Research, University of Missouri-Rolla, Rolla, Missouri 65401-0010

The influence of an applied microwave field on the dynamics of methylamine-dichloromethane (DCM) mixtures bound within atactic polystyrene (*a*-PS) over a range of polymer densities from 30 to 94 wt % polymer was examined using atomistic molecular dynamics simulations. This study is an extension of previous studies on methylamine transport in relatively polar polystyrene solutions of methanol and dimethylformamide [M. J. Purdue *et al.*, J. Chem. Phys. **124**, 204904 (2006)]. A direct comparison is made across the three types of polystyrene solutions. Consideration is given to both solvent and reagent transport within the polymer solutions under zero-field conditions and in an external electromagnetic field in the canonical ensemble (*NVT*) at 298.0 K. Various frequencies up to 10^4 GHz and a rms electric field intensity of 0.1 V/Å were applied. The simulation studies were validated by comparison of the simulated zero-field self-diffusion coefficients of DCM in *a*-PS with those obtained using pulsed-gradient spin-echo NMR spectrometry. Athermal effects of microwave fields on solute transport behavior within polymer solutions are discussed. © *2006 American Institute of Physics*. [DOI: 10.1063/1.2353112]

INTRODUCTION

A fundamental understanding of the molecular phenomena involved during the transport of key materials through polymeric media has long been considered a primary goal underpinning future advances in membrane separations, drug delivery systems, and organic synthesis. In particular, a quantitative description of solvent, solute, and/or reagent mobility in the polymer matrix at different levels of polymer density is paramount to the development of accurate macroscopic models of mass transport in the polymeric medium. Furthermore, methods that result in the selective enhancement of specific modes of transport or reaction pathways are at the forefront of research and include the tailoring of the polymer molecular structure to tune for solubility and kinetic selectivity and, more recently, the application of external microwave fields to influence selected transport processes and/or reactions. In the latter case an understanding of the mechanistic interaction of microwave fields with the systems under consideration is of major importance to the development of novel separation technologies,[2,3] heterogeneous catalysis,[4,5] and in solid phase organic synthesis (SPOS).[6–8] Selective desorption of polar species from catalyst sites using microwave fields was investigated in Ref. 4 to reduce the extent of catalyst deactivation due to a coking process. Optimization of reaction conditions for SPOS has been undertaken in Ref. 7 using a design of experiment approach. Reaction time, temperature, and reagent concentration were the key factors to obtain enhanced reaction times of 30 min against 48 h with conventional heating techniques. Likewise, improvements in reaction times from a minimum of 24 h to days under conventional conditions to 5 min of reaction under microwave heating conditions with yields exceeding 95% were explored in Ref. 8. A detailed physical understanding of the underlying mechanisms for such rate enhancements remains elusive and is part of the scope of this research.

An important point to establish when performing research on microwave effects is whether the thermal conditions with microwave heating are identical to conventional heating techniques, such that differences in the experimental or simulated responses to those under field-free conditions can be appropriately attributed to nonthermal phenomena. Temperature control is critical to reproducibility of experiments in SPOS, particularly when transferring chemistry from monomode to multimode microwave ovens.[9] The results in Ref. 9 demonstrate reproducibility of results using multiwell plates rotated in a multimode cavity, where the temperature of the reactor unit was controlled by a fiber-optic sensor to within 1 °C precision. Such technology permits uniform and identical heating of parallel reactions relative to sequential reactions in monomode cavities. However, in order to progress the understanding of microwave effects, accurate and direct temperature control close to the reaction sites must be utilized. An infrared (IR) pyrometer was used to control the temperature in Ref. 4 to minimize thermal

---

[a] Author to whom correspondence should be addressed. Fax: 353-1-7161177; Electronic mail: don.macelroy@ucd.ie

gradients within the catalyst bed. In this study, nonthermal effects were associated with the selective rotational excitement of adsorbed phenol groups such that enhanced desorption of loosely bound phenol groups was established. In an earlier study, microwave enhanced diffusion of ethylene oxide (EO) in polyvinylchloride (PVC) was examined by means of a microwave desorption apparatus, useful for removing toxic EO in polymeric medical supplies.[10] By comparison between conventional and microwave enhanced desorption of EO, it was found that microwaves reduce the desorption time by 250%–450%. Using an Arrhenius description of the temperature dependence of penetrant mobility, a significant reduction in the activation energy was found using microwave heating compared to conventional heating. The reduction was of the order of the translational kinetic energy of the diffusant molecules in the field-on environment. An increase in the fraction of mobile penetrants was accounted for by the active disruption of the EO/PVC hydrogen bonding. A twofold increase in diffusion of EO in PVC under field-applied conditions relative to zero-field conditions at the same temperature was determined in most cases. The rapid volumetric heating that microwave heating offers has been acknowledged, but it is worth investigating the molecular dynamics responsible for a further increase in molecular mobility relative to field-free conditions.

The aim of the current research is to observe similar phenomena in polystyrene solutions from a computational standpoint utilizing a range of field frequencies in order to elucidate a physical understanding of such observations. Current simulations with an order of 10^4 molecules required a high rms electric field strength of 0.1 V/Å in order to observe microwave effects within accessible simulation periods. A Nosé-Hoover chain of five thermostats was applied throughout the simulations to eliminate heating effects. There are currently no known experimental observations corresponding to the field-applied simulated results reported in this study. In a recent paper, theoretical results were reported for methanol (solvent) or dimethylformamide (DMF) (solvent) and methylamine (dilute reagent) in atactic-polystyrene (*a*-PS) using molecular dynamics simulation techniques.[1] In that study molecular mobility enhancement due to microwave field interaction with these polar solvent SPOS mixtures over a wide range of *a*-PS densities was of primary concern. In this paper we report computational results for a system containing a solvent which is far less polar than either methanol or DMF, namely, dichloromethane (DCM)/methylamine/*a*-PS solutions, and comparisons across the three different solvent types are made. All of the simulated individual polymer solutions considered herein involve a single solvent type, with a single methylamine reagent and no ionic additives.

SIMULATION METHODS

The five-site fully atomistic model of Ferrario and Evans[11] and the four-site united atom model of Impey *et al.*[12] were employed for solvent DCM and reagent methylamine, respectively. These potential models have been previously combined in the work of Impey *et al.* and employ a 12-6

TABLE I. Dicholoromethane atomic force field parameters at λ=1.

Atom	ϵ/k_B (K)	σ (Å)	q (e)[a]
C	51.0	3.35	0.022
Cl	175.0	3.35	−0.109
H	13.4	2.75	0.098

[a]$e \approx 1.6022 \times 10^{-19}$ C.

Lennard-Jones potential function and a Coulombic interaction governed by sets of fixed partial charges located at the center of the atomic nuclei. A harmonic bond angle bending potential function was superimposed on these models. The spring constants and equilibrium bond angles were taken from the parm99 version of the AMBER force field. As with previous studies of *a*-PS solutions using cubic periodic boundary conditions,[1] the initial polymer configurations were generated using POLYPACK software[13] and three configurations with nine chains of 40 monomeric units were generated using this noncommercial software package over a range of densities with simulation cell sizes up to 60 Å in length. In addition, the united atom molecular dynamics (MD) force field of Mondello *et al.*[14] was implemented so that the polymer contained no atomic charge sites and therefore remained inert to the external electromagnetic (e/m) field. The decision for using such a force field has been discussed in the previous studies[1] and is based on experimental evidence in Ref. 3. The structure of *a*-PS using this polymer potential model and a full description of the potential models for methanol and DMF have also been discussed in the previous work with *a*-PS solutions.

The cutoff radius for Lennard-Jones (LJ) interactions within either the liquid or polymer components was set at 10.5 Å and the Lorentz-Berthelot mixing rules[15] were applied for interactions between different types of LJ sites within the same or across different components. All MD simulations were performed at constant volume using a Nosé-Hoover chain of five thermostats with a fluctuation period of 0.5 ps. The time evolution of the solvent/reagent/polystyrene component and solution temperatures were monitored over the course of the simulations to verify that no heating effects occurred and a field-on equilibrium was established. A simple Coulombic potential was used in the simulations of polystyrene solutions presented herein, applying the nearest image convention for electrostatic interactions of the penetrant species. As discussed in Ref. 1, the truncation error associated with the nearest image convention at all of the simulated polymer densities was determined to be minimal based on comparisons of the molecular mean squared displacement between results with and without long-range electrostatic interactions using the Lekner summation method[16] at the highest simulated polymer density. The nonbonded force field parameters for DCM are shown in Table I. The intramolecular force field parameters in DCM consisted of equilibrium angles of 109.47° to produce a tetrahedral geometry, a harmonic spring constant of 35 kcal/mol for the H–C–H bond angle, and a harmonic spring constant of 50 kcal/mol for each of the remaining five bond angles.

The method used to solvate the *a*-PS samples and obtain

the partition coefficient K has been detailed previously in order to balance the solvent excess chemical potential with the bulk liquid solvent at thermal and mechanical equilibria.[17] The method involves a scaling parameter λ to slowly reduce the particle radii of the nonhydrogen atoms towards a noble state and the LJ well depth of the hydrogen atoms to zero. The same scaling relations for the three types of atoms relevant to this method are used as before[1] with an atomic radius reduction factor for DCM of $f_{RD}=0.9$. Each polymer solution was subsequently equilibrated for 10 ps in the appropriate e/m field environment, followed by a production period of 400 ps. A single time step scheme was used with steps of 1.0 fs over the course of all the simulations. In addition, the incorporation of the e/m field was implemented in the same manner as in Ref. 1 with the methanol/a-PS and DMF/a-PS solutions. Specifically, a plane polarized alternating monochromatic e/m field was applied uniaxially in the z direction. The electromagnetic force acting upon a charge site was superimposed upon forces that are accounted for under field-free conditions using a modified velocity Verlet algorithm,[18] where it has been shown that the effect of the magnetic component of the e/m field offers only a minor contribution to the net e/m force upon the charge site. A rms electric field strength of 0.1 V/Å was used to directly compare against the results for the previous polymer solutions under the same e/m field conditions.

Diffusion in polymers

The self-diffusion coefficients of DCM and methylamine were determined using the following generic model for the mean squared displacement (MSD) of the penetrant molecular center of mass, applicable when approaching the long-time Fickian diffusion regime from the anomalous regime:

$$\langle \Delta \mathbf{r}^2(t) \rangle = \frac{1}{N} \sum_i |\mathbf{r}_i(t) - \mathbf{r}_i(0)|^2 = At + B\sqrt{t}, \qquad (1)$$

where the parameter $A(\text{Å}^2/\text{ps}) = (3/5)D(10^{-9} \text{ m}^2/\text{s})$. This model was chosen as the optimum choice to use on the basis of an overview analysis of contemporary simulation results.[1] Translational mobilities were compared against two phenomenological descriptions of diffusion in polymers, namely, the free volume theory of Vrentas and Duda[19] and the parameter-free Mackie-Meares lattice model.[20] In the former model, the solvent self-diffusion coefficient in a solvent(1)/polymer(2) system can be written as

$$\frac{(1 - \omega_1)}{\ln(D_1/D_B)} = A' \omega_1 + B' \quad (\text{constant } T), \qquad (2)$$

where the solvent self-diffusion coefficient D has been normalized by the solvent self-diffusion coefficient in the bulk liquid phase D_B. The second model is based on simple geometric hindrance

$$\frac{D_1}{D_B} = \left(\frac{1 - \Phi}{1 + \Phi} \right)^2, \qquad (3)$$

where Φ is the polymer volume fraction.

Solvent and reagent rotational motion

The mean squared angular displacement (MSAD) of the molecular dipole moment vector of solvent or reagent is the rotational analog to the MSD for translational molecular motion. Let $\mathbf{r}_{ab} = x_{ab}\mathbf{i} + y_{ab}\mathbf{j} + z_{ab}\mathbf{k}$ denote a vector in Cartesian coordinates between points a and b in a molecule. The angular displacement of this vector is written as follows:

$$
\begin{aligned}
\theta^{ab} &= \Delta\theta_x^{ab}\mathbf{i} + \Delta\theta_y^{ab}\mathbf{j} + \Delta\theta_z^{ab}\mathbf{k} = [\theta_x^{ab}(t + \Delta t) - \theta_x^{ab}(t)]\mathbf{i} \\
&\quad + [\theta_y^{ab}(t + \Delta t) - \theta_y^{ab}(t)]\mathbf{j} + [\theta_z^{ab}(t + \Delta t) - \theta_z^{ab}(t)]\mathbf{k} \\
&= \left[\cos^{-1}\left(\frac{x_{ab}(t + \Delta t)}{|\mathbf{r}_{ab}|} \right) - \cos^{-1}\left(\frac{x_{ab}(t)}{|\mathbf{r}_{ab}|} \right) \right]\mathbf{i} \\
&\quad + \left[\cos^{-1}\left(\frac{y_{ab}(t + \Delta t)}{|\mathbf{r}_{ab}|} \right) - \cos^{-1}\left(\frac{y_{ab}(t)}{|\mathbf{r}_{ab}|} \right) \right]\mathbf{j} \\
&\quad + \left[\cos^{-1}\left(\frac{z_{ab}(t + \Delta t)}{|\mathbf{r}_{ab}|} \right) - \cos^{-1}\left(\frac{z_{ab}(t)}{|\mathbf{r}_{ab}|} \right) \right]\mathbf{k}. \qquad (4)
\end{aligned}
$$

Equation (4) can be used to compute the angular displacement of a molecule i in a time interval of Δt. The cumulative angular displacement can then be used to compute the mean squared angular displacement. The angular velocity of the a-b vector in molecule i at time $t + \Delta t$ is given as follows:

$$\omega_i^{ab}(t) = \dot{\theta}_i^{ab}(t) = \left(\frac{\Delta\theta_x^{ab}}{\Delta t} \right)\mathbf{i} + \left(\frac{\Delta\theta_y^{ab}}{\Delta t} \right)\mathbf{j} + \left(\frac{\Delta\theta_z^{ab}}{\Delta t} \right)\mathbf{k}. \quad (5)$$

Equation (5) can be applied to the angular velocity of the dipole moment vector of a molecule. The normalized molecular dipole angular velocity autocorrelation function (ACF) is written as follows:

$$c_{\omega\omega}(t) = \frac{\langle \omega_i(t) \cdot \omega_i(0) \rangle}{\langle \omega_i(0) \cdot \omega_i(0) \rangle}, \qquad (6)$$

where ω_i represents the angular velocity of the electric dipole moment vector of solvent molecule i. Equation (6) shall be used to compare the angular motion of the three different solvents in a-PS across a range of e/m field frequencies at a fixed polymer density.

RESULTS

Equilibration of polymer solutions

Table II shows numerical values of the equilibrium weight percentage of DCM and solvent particle number N obtained for equilibrated DCM/a-PS solutions using the technique described in Ref. 17. These results represent averages over three independent configurations at each polymer density. A smooth decay of the partition coefficient for DCM/a-PS solutions was found using these data.[21]

Validation of zero-field dynamical simulation results for DCM and DCM/a-PS mixtures

Bulk liquid simulations involved 256 molecules using a simulation time of 600 ps in the NVT ensemble at 25 °C. The time averaged molecular electric dipole moments of DCM were determined to be 1.66 D. The gas phase electric dipole moment of DCM is 1.6 D. By comparison with the

TABLE II. Dichlormethane in atactic polystyrene at 298 K.

L (Å)	Polymer density (g/cm^3)	Φ	wt. DCM (%)	N_{DCM}
40	0.97	0.60	6.1	29
45	0.68	0.42	38.8	280
50	0.50	0.31	57.6	523
55	0.37	0.23	69.8	1020

TABLE III. DCM Arrhenius parameters: preexponential factors D_0 (m^2/s) and activation energies E_D (J).

	$D_0/10^{-7}$ (m^2/s)	$E_D/10^{-20}$ (J)
Wike-Chang	2.34	1.72
MTS^3	1.19	1.53
MTS^2	1.40	1.59

corresponding molecular dipole moments in Ref. 1 for liquid methanol (2.25 D) and liquid DMF (4.33 D), liquid DCM is relatively nonpolar and its polarity is closest to that of liquid methylamine (1.30 D) at −23 °C. Since methylamine boils at −6.4 °C, the simulation temperature for pure liquid methylamine was chosen for comparison with the results of Impey *et al.*[12] The computed liquid phase dipole moment of methylamine is very close to the gas phase value of 1.31 D.

Evidence of strong Arrhenius diffusive behavior, conforming to a Wilke-Chang empirical fit[22] is shown in Fig. 1(a) for bulk liquid DCM over a range of temperatures. MTS^2 and MTS^3 denote two- and three-tiered multiple time step schemes.[23] Internal molecular motion in the MTS^2 scheme allows bond angle bending but constrains bond lengths with the RATTLE algorithm.[24] The MTS^3 scheme has the additional feature of bond length flexibility and as before the harmonic spring constants were obtained with the parm99 version of AMBER. The MTS^2 scheme performs slightly better than the MTS^3 scheme when comparing simulation results against the Wilke-Chang empirical fit. Table III contains values of the preexponential factors and activation energies determined using the simple Arrhenius relationship $D=D_0 e^{-E_D/k_B T}$, where k_B is Boltzmann's constant. A mutual diffusion coefficient for methylamine in DCM of 2.3×10^{-9} m^2/s was determined, compared to a Wilke-Chang value of 2.8×10^{-9} m^2/s.

The mobility of bulk methanol and DMF at 25 °C in external e/m fields has been previously studied using a rms electric field intensity of 0.1 V/Å. Both of these solvents indicated a local maximum in their mobility at about 100 GHz. It is of interest here to compare the behavior of bulk liquid DCM at 25 °C in the same e/m field environments. Figure 1(b) illustrates the mobility of these three solvents relative to their zero-field self-diffusion coefficients. The curves represent guides to the eyes and it is apparent that there is no local maximum in the mobility of DCM up to and including 2000 GHz, but instead DCM shows a monotonic increase in mobility. The enhancement of DMF mobility is greatest and the enhancement of methanol mobility is smallest.

Using the intercept values from Eq. (1) to obtain estimates of penetrant diffusion coefficients, the simulated self-diffusion coefficients of DCM in *a*-PS at 25 °C were compared against experimental values over a range of solvent weight fractions ω_1 in Fig. 2. (Zero-field simulation results for translational and rotational diffusion coefficients for DCM and methylamine are provided in Tables IV–VII.) The experimental diffusion coefficients were obtained using pulsed-gradient spin-echo NMR spectrometry. There were technical difficulties in obtaining accurate pure liquid DCM self-diffusion coefficients at $\omega_1=1$ and therefore the experimental value for pure bulk DCM is not shown. The linear trend that is apparent with the experimental data can be extrapolated to a value at $\omega_1=1$ of 3.7×10^{-9} m^2/s, which is only slightly greater than the Wilke-Chang value in Fig. 1(a)
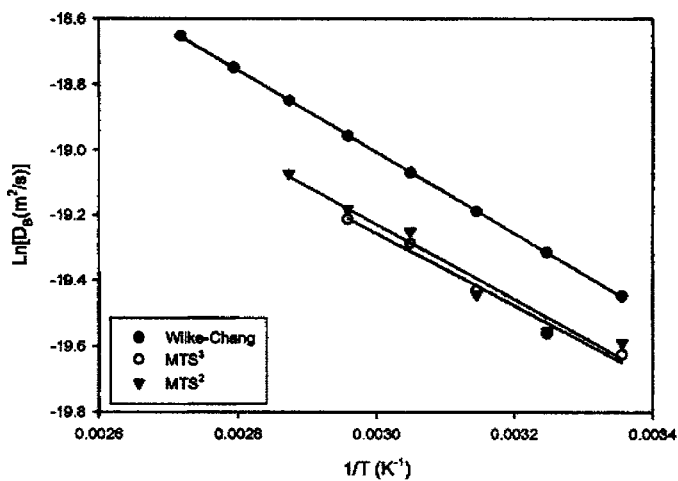
(a)
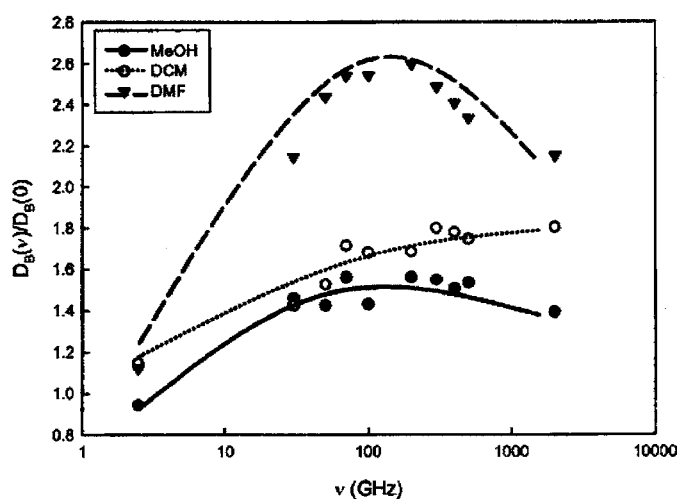
(b)

FIG. 1. Dynamics of bulk liquid solvents at 25 °C using the Lekner summation method: (a) Arrhenius plot of zero-field self-diffusion coefficient in liquid dichloromethane. (b) Variation of solvent mobility relative to the zero-field solvent self-diffusivity with the frequency of an externally applied e/m field (rms electric field strength of 0.1 V/Å).
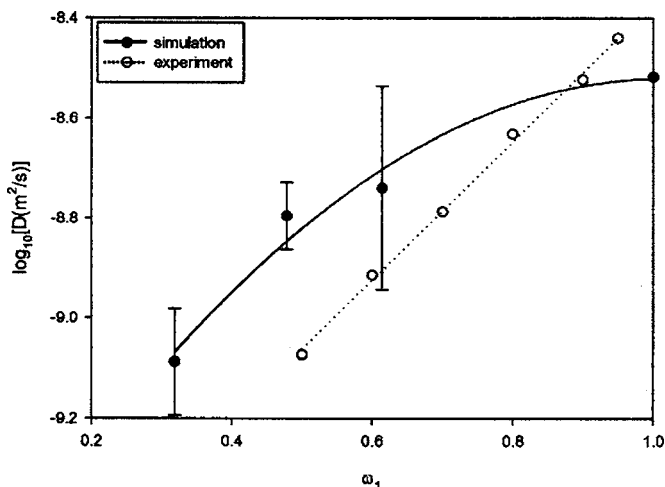
FIG. 2. Comparison of the simulated zero-field self-diffusion coefficient of dichloromethane in a-PS solutions with experimental values determined using pulsed-gradient spin-echo NMR spectrometry over a range of solvent weight fractions at 25 °C.

of 3.6×10^{-9} m^2/s and in turn is greater than the simulated result of 3.1×10^{-9} m^2/s. Since the polymer force field is of no consequence for pure solvent simulations, the disparity between simulation and experiment in this case is believed to be attributable to discrepancies embedded in the solvent force field employed in the simulations.

As with previous simulations with DMF in a-PS,[1] the discrepancy between simulation and experiment is most pronounced at low solvent weight fractions where polymer-solvent interactions are reduced. Solvent diffusion is therefore overpredicted, which can be attributed to three main factors associated with the simulated results: (i) a weak force field (shifted force LJ potential and no electrostatics on polymer) that underestimates the strength of the interactions between solvent and polymer, (ii) use of finite molecular weight chains, and (iii) united atom groups on polymer. Such limitations are related to the size of the simulation cell and the available computational power. However, these zero-field results support the combined use of the chosen DCM and a-PS potential models and provide a basis for the forthcoming results with an externally applied e/m field.

Structure and dynamics of solvent/a-PS mixtures under zero-field conditions

Figure 3 illustrates the intermolecular separation of the solvent center of mass (COM) from side phenyl group centers (by mass) and backbone carbon triplets over a range of box sizes. The corresponding polymer densities are reported in Table II. A clear reduction in liquid-polymer structure can be seen as the polymer density is reduced. By comparison

TABLE V. Methylamine mobility (m^2/s $\times 10^{-9}$) under zero-field conditions in methylamine/dichloromethane/a-PS solutions at 25 °C.

$L(A)$	A	B	C	Average
45	0.707	2.540	0.138	1.129
50	2.321	2.133	0.000	1.485
55	3.047	5.586	1.426	3.353

with methanol/a-PS solutions, the structure of DCM and DMF to a-PS moieties is more defined. This is due to the larger solvent DCM and DMF molecules that have restricted access to phenyl and backbone moieties. Thus, methanol may permeate a-PS without necessitating rotational motion. Figures 3(c) and 3(d) for DMF/a-PS solutions are similar to Figs. 3(e) and 3(f) for DCM/a-PS solutions, but the population of the second solvation shell of DMF about the backbone is not higher than the first shell at the highest polymer density. The polymer backbone is therefore more accessible to DMF than to DCM, which is believed to be due to the anisotropic geometry of the DMF molecule. With suitable reorientation of the planar molecule, DMF can pass through narrow voids close to the polymer backbone.

For the three solvent types, methanol can access the most configurations within the a-PS solution, DMF may access restricted regions with suitable reorientation, and DCM is most restricted in its sampling space. By comparison to the bulk liquid, DCM in a-PS solutions is relatively confined and may be compared to regular close packed spinning tops which may or may not cooperate. The trends observed in the structure of the a-PS solutions are expected to influence the resulting trends observed in the molecular dynamics. The solvent molecular dipole ACF has been previously examined for methanol and DMF in e/m fields over a range of e/m field frequencies.[1] A comparison of the molecular dipole angular velocity ACF of methanol, DMF, and DCM at a single polymer density of 0.5 g/cm^3 is considered in Fig. 4, as determined using Eq. (6). In Fig. 4(a), the most rapid decay of this ACF is observed for solvent methanol, which primarily occurs within 0.5 ps. In Fig. 4(b), the DMF molecular dipole angular velocity ACF indicates a period of time between 1 and 2 ps when its angular motion is interrupted over the sampling period. This extended interruption to angular motion can be associated with DMF/a-PS interactions, such as those encountered with restrictions from the polymer backbone. The decay behavior is therefore relatively long lived as DMF molecules navigate the interstices of a-PS. A degree of symmetry in the dynamics of solvent DMF was found in the hydrogen atom velocity autocorrelation functions (VACFs) and the neighboring C–O bond angular VACF.[21] In Fig. 4(c), there is a strong degree of symmetry present in the rapid

TABLE IV. DCM mobility (m^2/s $\times 10^{-9}$) under zero-field conditions in methylamine/dichloromethane/a-PS solutions at 25 °C.

$L(A)$	A	B	C	Average
45	0.738	0.825	0.898	0.821
50	1.572	1.719	1.525	1.605
55	1.483	1.902	2.149	1.845

TABLE VI. DCM molecular dipole orientations rotational diffusion coefficient $D_{R,\text{orient\_dip},1}$(v) (ps^{-1}) in methylamine/DCM/a-PS solutions at 25 °.

$L(A)$	A	B	C	Average
45	0.339	0.345	0.338	0.340
50	0.354	0.354	0.347	0.352
55	0.293	0.344	0.337	0.325

TABLE VII. Methylamine molecular dipole orientation rotational diffusion coefficient $D_{R,\text{orient\_dip},1}(v)$ (ps^{-1}) in methylamine/DCM/a-PS solutions at 25 °C.

$L(A)$	A	B	C	Average
45	1.329	1.137	1.139	1.201
50	1.230	1.382	1.217	1.277
55	0.713	1.134	1.243	1.030

decay behavior of the ACF for DCM, which can be attributed to the tetrahedral geometry with restricted access to the polymer backbone. These dynamical results are supported by the structural results obtained with the radial distribution function (RDF) analysis in Fig. 3.

Translational molecular motion of methylamine/DCM/ *a*-PS mixtures in external electromagnetic fields

The self-diffusion coefficients or mobilities of DCM and methylamine were determined using Eq. (1), after establishing the behavior of $d(\log\langle\Delta r^2\rangle)/d\log(t)$ over the course of the sampling period of 100 ps, and applying the generic correlation to data outside the early time ballistic regime. The dependence of DCM and methylamine transport on microwave field frequency and polymer density is depicted in Fig. 5. These figures are based on an averaging of diffusion results from three selected polystyrene configurations at each density shown in Table II. The error bars at each density represent the error bounds on the averaged results at the 95% confidence level from samples of three independent configurations. The curves show general trends that indicate how the e/m field affects the solvent or reagent relative to the same polymer solutions under zero-field conditions. Fickian diffusion of DCM was not approached in the highest density systems and therefore no mobility results have been included for these systems in Fig. 5. It is apparent from Fig. 5 that there is very little dependence of DCM mobility enhancement on polymer density and is related to the fact that DCM cannot easily penetrate the interstices of *a*-PS. As with methylamine/DMF/*a*-PS solutions, the external microwave field induces the greatest enhancement of methylamine and DCM mobility relative to diffusion in the polymer under zero-field conditions at 1000 GHz. Referring to Fig. 1(b), the enhancement factor for DCM is about 30% larger in the bulk liquid phase at 1000 GHz. There is no significant mobility enhancement of DCM in *a*-PS at 10^4 GHz.

In Figs. 6(a) and 6(b), DCM self-diffusion coefficients in *a*-PS are normalized by the corresponding values in the bulk liquid phase (to which quasiequilibrium has been established) under identical field conditions and each curve can be distinguished by e/m frequency. In Fig. 6(a), the curves represent guides to the eyes. In Fig. 6(b), the curves are fitted using a quadratic polynomial. Figure 6(a) illustrates the effect of the solvent loading on solvent mobility (in validating the Vrentas-Duda model) in different e/m fields and shows how the model of penetrant diffusion for DCM is not adhered to under zero-field and field-applied conditions using the simulated data. This phenomenological description was approached under conditions of zero-field or very high field

frequencies for methanol in *a*-PS but not for DMF.[1] It may be observed from Fig. 6(a) that the e/m field induces a parametric separation of polar penetrant mobilities against different solvent weight fractions. Figure 6(b) illustrates the effect of the polymer on solvent mobility in different e/m fields. As with previous simulations of methanol/*a*-PS solutions,[1] the curve for 10^4 GHz is highest in Fig. 6(b), which contrasts with the situation for DMF/*a*-PS solutions[1] where it is lowest at 10^4 GHz. All results lie above the parameter-free Mackie-Meares model, representing the motion of a nonpolar solvent in *a*-PS under all field conditions. It is apparent therefore that the external e/m field induces a parametric separation of polar penetrant mobilities above a level corresponding to simple geometric hindrance by the polymer. Since the enhancement of DCM mobility by an applied e/m field is largely independent of polymer density [refer to Fig. 5(b)], the shape of each curve in Fig. 6(b) closely corresponds to the shape of the zero-field curve. In all cases, as with DMF/ *a*-PS solutions, the ordinate remains below unity [such that the ordinate for Fig. 6(a) is necessarily negative] and therefore diffusion of DCM is hindered by the presence of *a*-PS.

In Fig. 7(a), the intermolecular chlorine-hydrogen structure in DCM bound within *a*-PS decreases with increasing frequency up to 1000 GHz. Unlike DMF, the suppression of rotation of the DCM molecular dipole at 10^4 GHz does not inhibit translation on account of molecular symmetry. The structure of the solvent in *a*-PS therefore reverts to its zero-field state. The second intermolecular solvation shell in Fig. 7(a) appears to be unaffected by a change in frequency. The squared displacement between successive jumps, r_p^2, was computed between successive positional averages with 1.0 ps intervals. Temporal jump maps for the reagent were also examined[21] and consisted of examining the time dependence of r_p^2 to identify a typical jump mechanism of penetrant motion in polymers. In Fig. 7(b), reagent jump lengths can be seen to be greatest at 1000 GHz, although the scale of these jumps is about 60% of those in methylamine/methanol/ *a*-PS solutions at the same density and field conditions. The curves in Fig. 7(b) represent guides to the eyes. The difference in the magnitude of the jumps is expected considering that the molecular weight of methanol (32.04 g/mol) is less than half of that of DCM (84.93 g/mol) and that the molecular weight of methylamine is far closer to that of methanol.

The orientation of solvent molecular dipoles relative to the COM of the methylamine reagent has been illustrated and discussed in the previous simulations with methanol and DMF in *a*-PS. The residence time distribution (RTD) of the solvent within a 6.5 Å cosphere of the reagent has also been obtained previously and a mean solvent residence time can subsequently be computed. In Fig. 8(a), the orientation of DCM in a 6.5 Å cosphere of the reagent can be seen to be most structured at 1000 GHz, corresponding to the frequency at which DCM mobility is most enhanced.

The effect of e/m field frequency on the RTD of DCM in a cosphere of methylamine is shown in Fig. 8(b). The initial ordering of the RTD with respect to frequency is the same as with the orientational distribution functions, indicating how the time averaged relative molecular orientations between solvent and reagent are closely related to the dynamics of
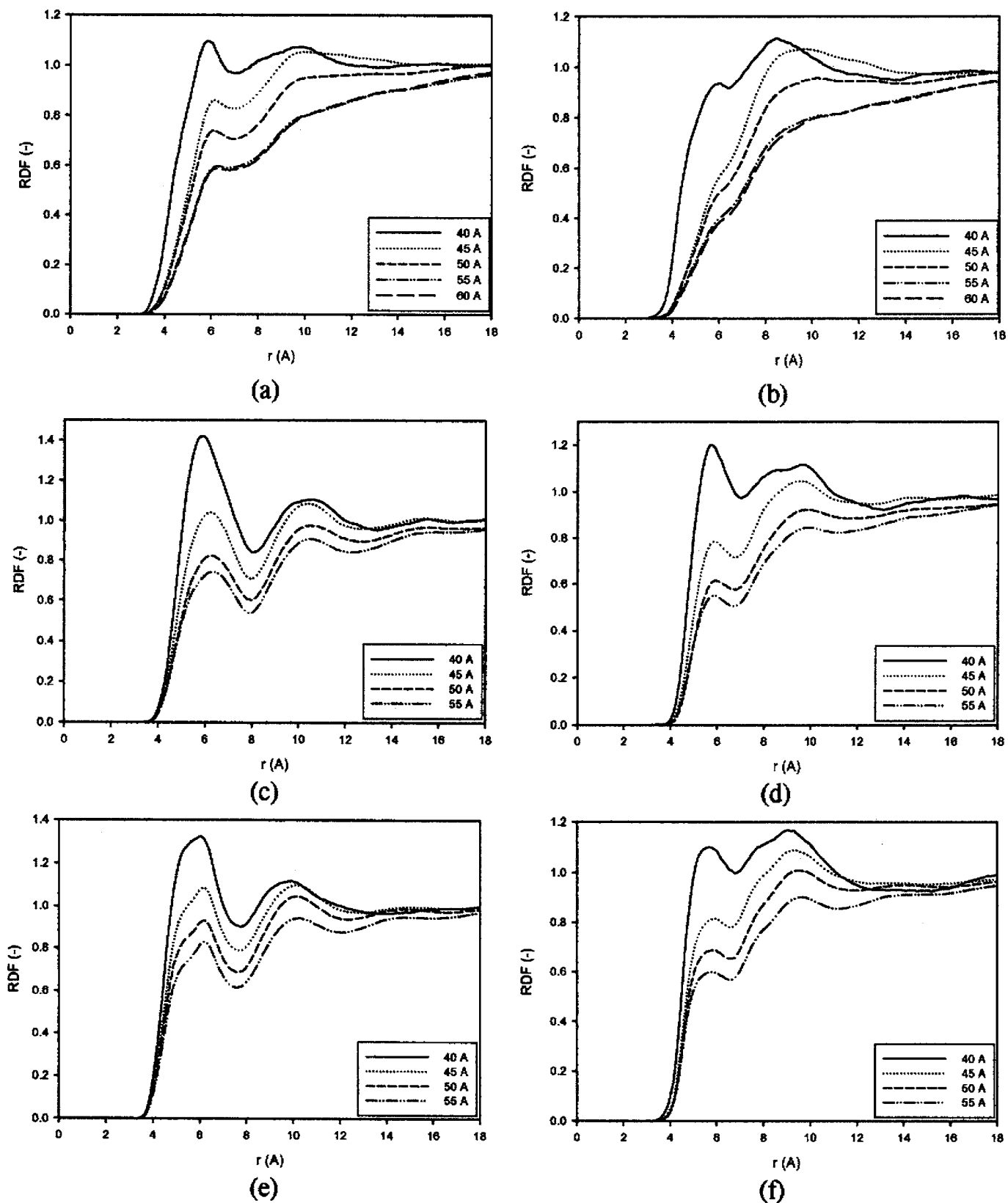
FIG. 3. Heteroatomic solvent COM-phenyl/C3b COM RDFs at 25 °C in methylamine/solvent/*a*-PS solutions over a range of simulation box sizes: (a) MeOH COM-phenyl group COM, (b) MeOH COM-C3b COM; (c) DMF COM-phenyl group COM, (d) DMF COM-C3b COM; (e) DCM COM-phenyl group COM, and (f) DCM COM-C3b COM.

solvent and reagent in contact. In broader terms, the rate at which neighboring solvent molecules within the cosphere of the reagent can cooperate efficiently with its translational motion depends on the structural organization of the solvent.

The computed mean residence times for DCM in a 6.5 Å cosphere of methylamine at an *a*-PS density of 0.5 g/cm³ were determined to be 2.87, 3.09, 2.62 and 2.28 ps at 0, 10^2, 10^3, and 10^4 GHz, respectively.
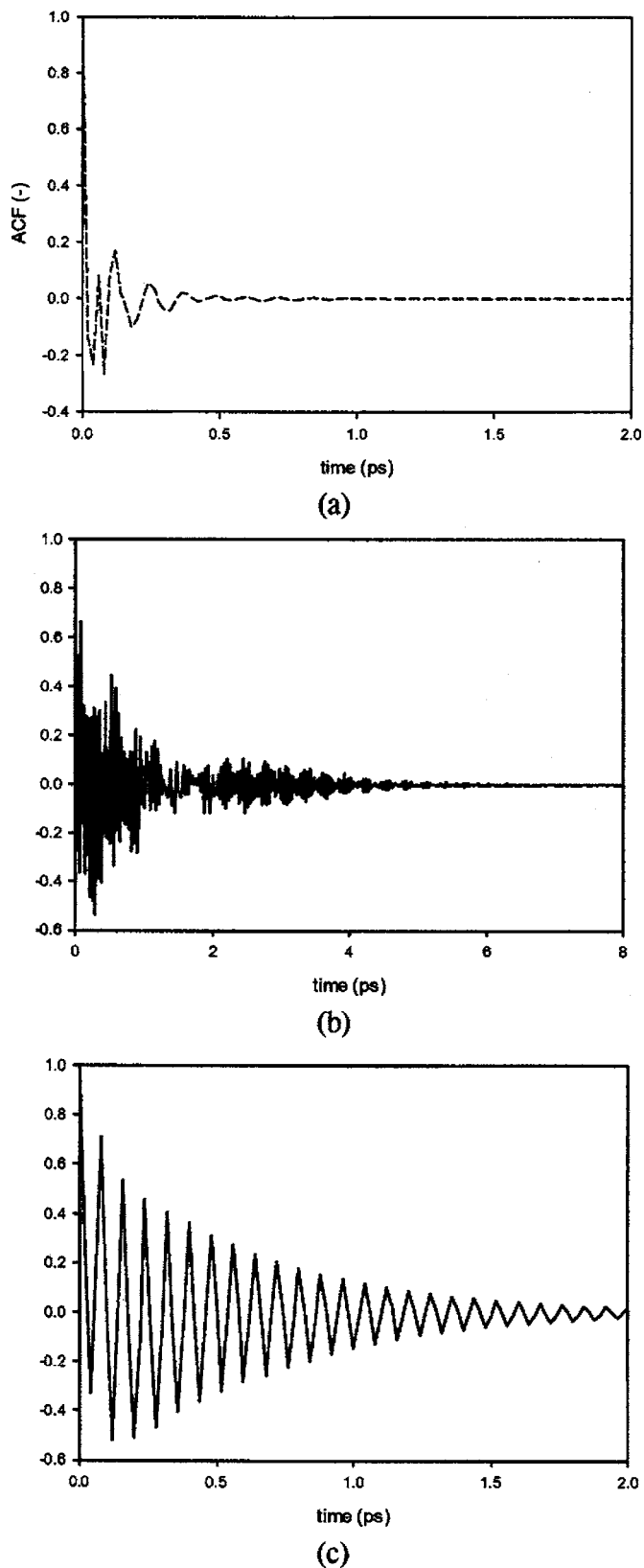
FIG. 4. Solvent molecular dipole angular velocity ACF at 25 °C in methylamine/solvent/*a*-PS solutions over a range of simulation box sizes: (a) MeOH, (b) DMF, and (c) DCM.

The molecular dipole moment ACFs for DCM over a range of e/m field frequencies at 25 °C and a polymer density of 0.5 g/cm^3 are shown in Fig. 9(a). The periodicity of the e/m field can be seen only at 1000 GHz over the sam-

pling period of 8 ps. A rapid decay of the ACF for DCM occurs at 100 GHz, but most notably the curves for zero-field conditions and at 10^4 GHz are coincident. The variation of the chlorine-hydrogen vector $c_2(t)$ ACF for DCM over the same range of conditions is displayed in Fig. 9(b), where the curves for zero-field conditions and at 10^4 GHz are again coincident. Due to the coincidence of translational and structural results at zero field and 10^4 GHz, it is instructive to examine the corresponding results with rotational molecular motion. Figure 10 illustrates the dependence of the molecular dipole orientation rotational diffusion coefficient of methylamine and DCM over a range of polymer densities and e/m field frequency and can be compared to those computed previously for methanol and DMF/*a*-PS solutions.[1] In Fig. 10(b), the variation of the enhancement in this DCM rotational diffusion coefficient closely resembles DCM mobility enhancement in Fig. 5(b), with an almost one-to-one enhancement correspondence. Intuitively, the tetrahedral symmetry of the DCM molecule provides little preference for rotational or translational motion. The e/m field therefore provides an unbiased enhancement of both dynamical modes unlike with methanol or DMF. The corresponding behavior for methylamine in Fig. 10(a) follows the opposite trend to DCM rotational mobility with e/m field frequency. Methylamine rotation therefore increases when DCM rotation decreases up to and including 10^4 GHz. However, based on the absolute values of the enhancement factors in Fig. 10, it is clear that the e/m field selectively enhances the rotation of methylamine to a greater extent than DCM.

The MSAD of both solvent and reagent in the direction of the electric component of the e/m field, corresponding to the *z* direction, is shown in Fig. 11. For the solvent, the MSAD was obtained by using Eq. (4) and averaging over all solvent molecules. In Figs. 11(a) and 11(b), it can be seen that rotational motion of methanol is below the zero-field level at 100 and 10^4 GHz but above it at 1000 GHz. The associated methylamine rotational motion is at the zero-field level at 100 GHz and above it at 1000 and 10^4 GHz. This indicates the selective rotational excitement of methylamine at 10^4 GHz in agreement with enhanced methylamine molecular dipole rotation and consequently enhanced translational mobility at this frequency.[1] In addition, the periodicity of the e/m field is apparent in the MSAD for methanol and methylamine at 100 and 1000 GHz, precisely when the Vrentas-Duda model of translational diffusion is invalidated.[1]

The periodicity of the e/m field can also be seen in the MSAD for both methylamine and DMF at 100 GHz in Figs. 11(c) and 11(d), respectively. It can be clearly seen that at 10^4 GHz, rotational motion of DMF is considerably reduced below the zero-field level, a feature that does not appear in Fig. 11(f) for DCM. In Fig. 11(c), the rotational motion of methylamine in DMF/*a*-PS solutions is at or below the zero-field level, without a sharp decrease in rotational mobility at 10^4 GHz. In addition, the rotational motions of methylamine and DMF occur to similar extents at 100 GHz and it is believed that a level of cooperation of the two species is responsible for enhanced reagent translational mobility at this frequency.[1] Therefore, since methylamine and DMF are of
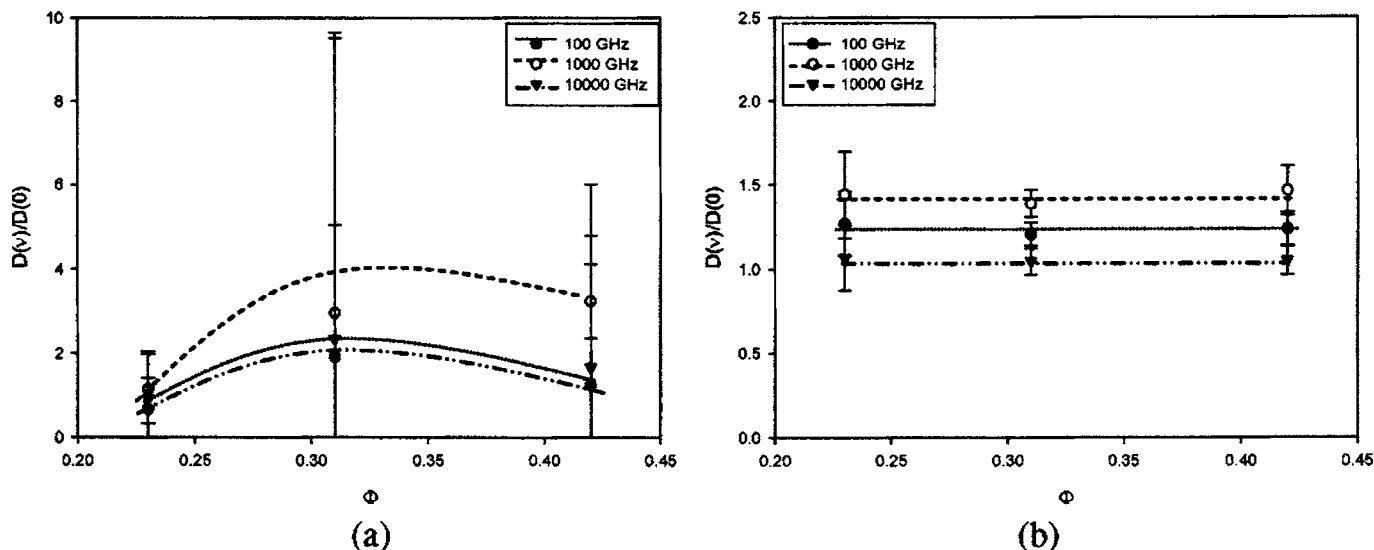
FIG. 5. Solvent/reagent mobility in methylamine/dichloromethane/a-PS solutions at 25 °C relative to zero-field conditions: (a) methylamine and (b) dichloromethane.

dissimilar sizes, enhancement of methylamine translational mobility is optimized when both species contain significant rotational mobility, in contrast to methanol/methylamine/a-PS solutions. The periodicity of the e/m field can also be seen in the MSAD for DCM at 100 GHz in Fig. 11(f). The rotational motion of DCM exhibits little noise through a regular and less chaotic motion that is apparent with the other polar solvents, methanol and DMF. Consequently, despite working in the Henry's law limit, the pattern of rotational motion of methylamine in DCM/a-PS solutions in Fig. 11(e) is also well structured and was found to occur to a slightly greater extent than DCM.

Local cooperative molecular motion as opposed to local competitive molecular motion based on *random* collisional interactions is expected to contribute significantly to observations of nonthermal microwave effects in condensed phases. Thermal effects of volumetric heating have long been

associated with random collisional interactions caused by dipolar oscillations as individual polar molecules align with the oscillating e/m field. Molecules which form localized clusters, assembled in part by the external field and based on a combination of polar and stereochemical interactions within a heterogeneous matrix, have been shown in this study to exhibit enhanced translational motion above that expected with random thermal effects. Such clusters contain an optimal number of molecules that can act to transform the supplied electromagnetic energy into translational solvent or reagent motion by adapting to the immediate environment. Population and structural changes in the cosphere of the reagent with e/m field frequency have been demonstrated in Fig. 8(a) and with previous work.[1] For methylamine/DCM/a-PS solution, the solvent population of the cosphere of the reagent drops with increasing DCM translation to coincide with increasing methylamine translation.
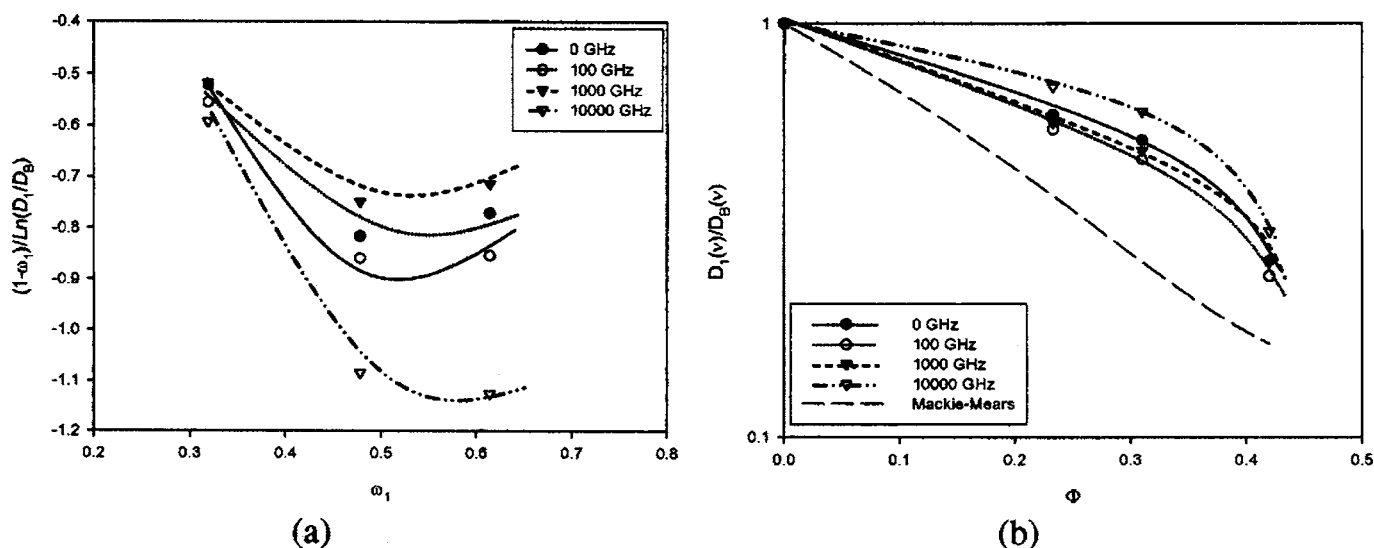

FIG. 6. DCM translational diffusivity (D_1) in methylamine/DCM/a-PS solutions at 25 °C over a range of frequencies and polymer densities and at a rms electric field intensity of 0.1 V/Å. (a) Validation of the Vrentas-Duda model [Eq. (2)]. (b) Self-diffusion relative to the bulk liquid under identical field conditions [the Mackie-Mears model is given by Eq. (3)].
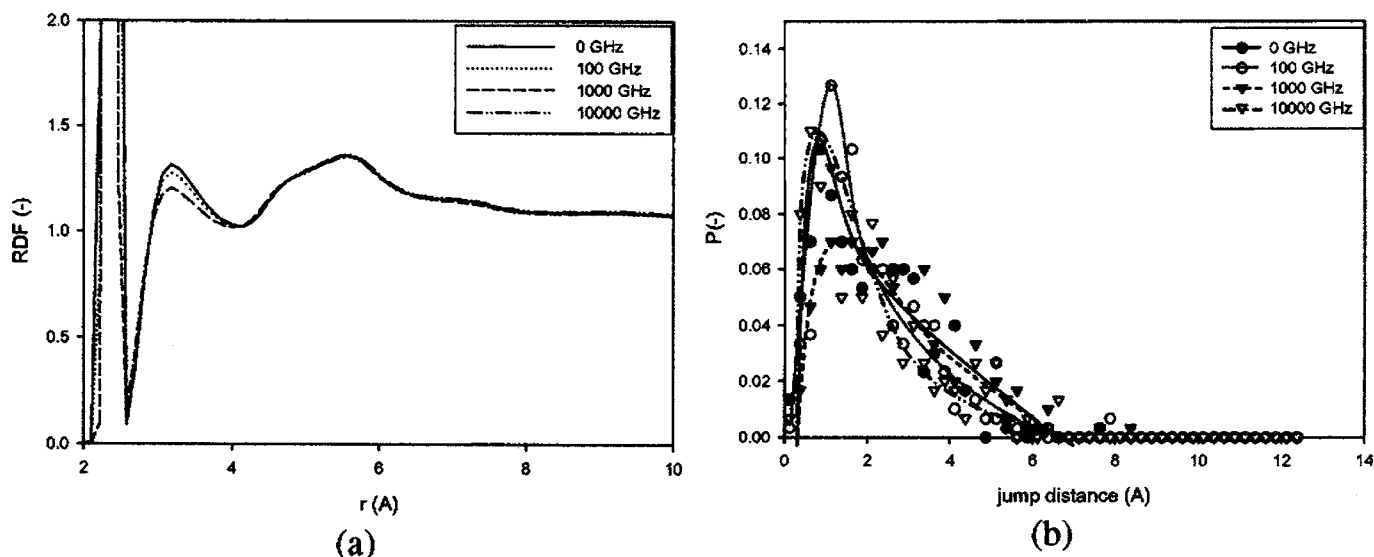
FIG. 7. Distribution functions at 25 °C in methylamine/dichloromethane/*a*-PS solutions (*a*-PS density=0.5 g/cm³) over a range of frequencies and a rms electric field intensity of 0.1 V/Å. (a) Heteroatomic DCM Cl-H RDF. (b) Jump length distribution of a single methylamine reagent.

The mode of operation of such a molecular cluster is critical to understanding how the parts of the cluster move relative to each other. In summary, polar methanol and methylamine are of similar molecular size. In this case, selective rotational excitement of methylamine, while retarding methanol, is responsible for a tunneling mechanism of diffusion. Polar DMF and methylamine are of dissimilar sizes and reagent translation is optimized by effective rotational cooperation rather than selective rotational excitement. Nonpolar DCM and methylamine behave differently in an e/m field. As the e/m field enhances DCM rotation, DCM and methylamine translation are both enhanced to different extents but methylamine rotation is suppressed. It may be concluded from this study that the optimal transport mechanism for the reagent occurs when both solvent and reagent rotational enhancements are similar such that the two species may effectively cooperate in a qualitatively similar manner as for me-

thylamine and DMF but largely independent of relative orientation. At this optimal frequency, methylamine in DCM/*a*-PS solutions is propelled efficiently within a close packed DCM cluster.

The optimal resonance frequencies of such molecular clusters in homogeneous or heterogeneous environments are not expected to correspond to individual molecular relaxation times. As an example, the optimal resonance frequency for bulk liquid methanol was not coincident with the O–H bond relaxation time, but clearly the enhancement in molecular mobility was related to this quantity.[1] By contrast with methanol or DMF, a maximum in the mobility enhancement of DCM was not observed in the bulk solvent. This contrast can be attributed to the regular molecular geometry and lack of association with DCM as opposed to the more polar solvents methanol and DMF. Figure 1(b) illustrates how the greatest enhancement of bulk solvent mobility occurs with
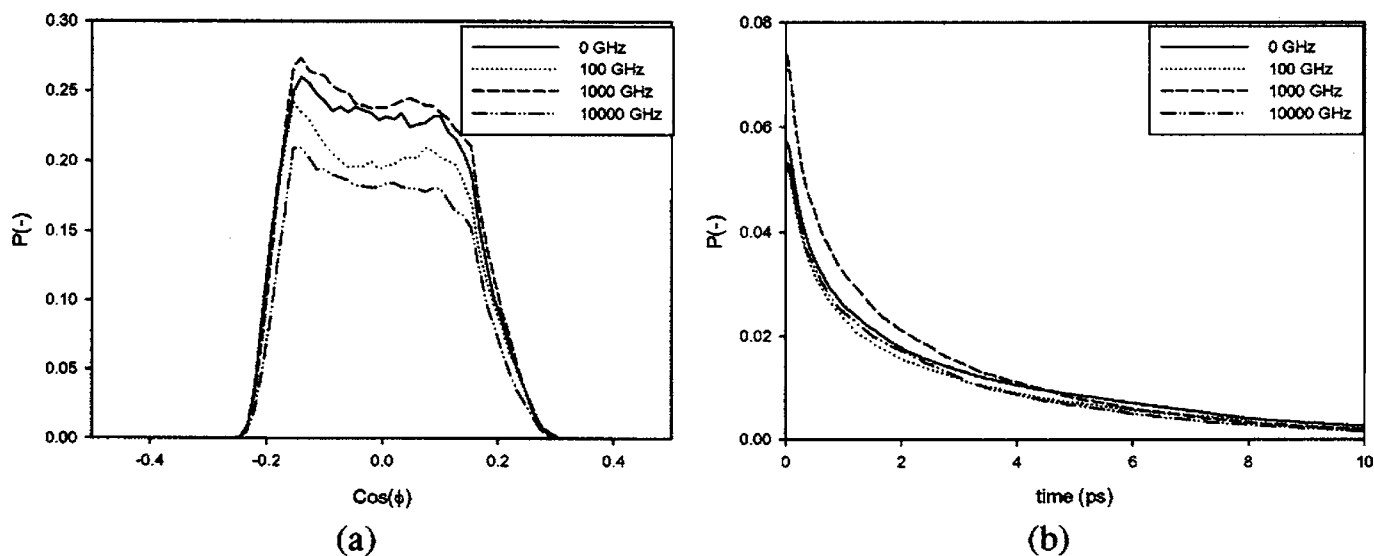

FIG. 8. Behavior of solvent DCM in a cosphere of a single methylamine reagent at 25 °C in methylamine/DCM/*a*-PS solutions (*a*-PS density=0.5 g/cm³) over a range of frequencies and a rms electric field intensity of 0.1 V/Å: (a) orientation of molecular dipole about methylamine and (b) RTD.
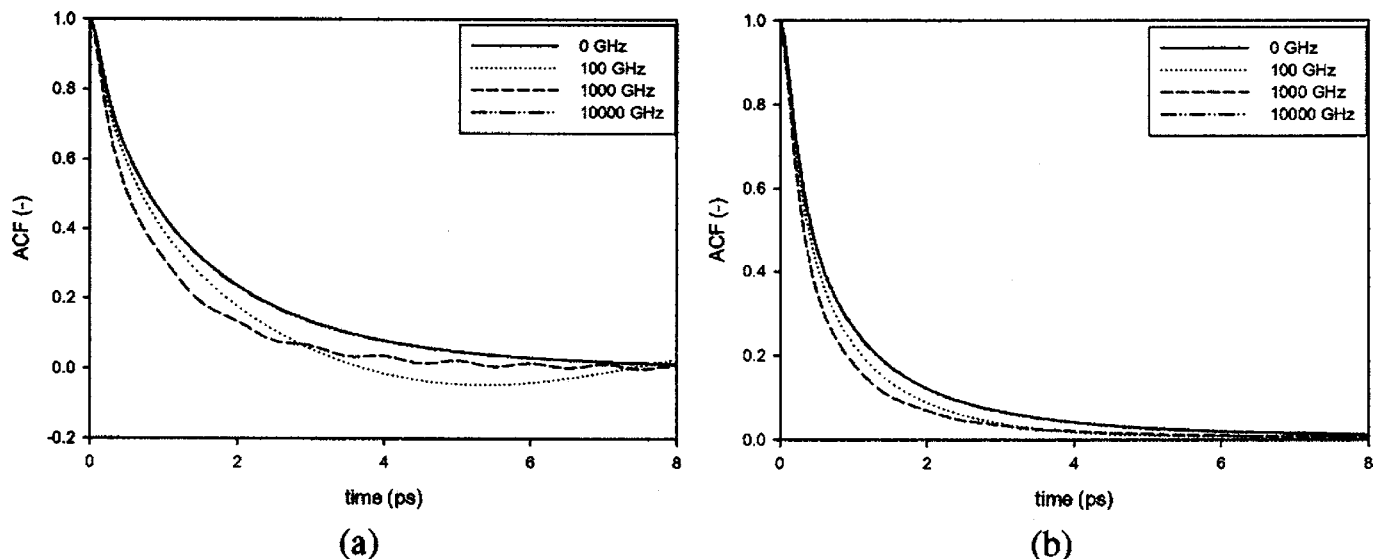
FIG. 9. Dichloromethane ACFs at 25 °C in methylamine/dichloromethane/*a*-PS solutions (*a*-PS density=0.5 g/cm³) over a range of frequencies and a rms electric field intensity of 0.1 V/Å: (a) molecular dipole and (b) $C_2(t)$ DCM Cl–H vector rotation.

DMF and the least enhancement occurs with methanol. However, once confined within *a*-PS, DCM did show an optimal resonance frequency, and additionally, its enhancement dropped below that of both methanol and DMF. Furthermore, the enhancement of methanol mobility in *a*-PS solutions was actually higher than the corresponding enhancement of DMF in *a*-PS. The extent of penetrant mobility enhancement in *a*-PS is therefore not only simply dependent on the polarity of the penetrant species but also on interactions within networks or units of molecules. In this case, methanol has the greatest potential to permeate the interstices of *a*-PS with suitable activation by the external e/m field, particularly since the hydrogen bonded network is disturbed by the presence of the polymer itself. The enhancement of methylamine translational mobility is of a similar order in all three *a*-PS solutions.[1] The molecular mobility enhancements that have been determined in this study are of the order that has been

determined experimentally for microwave enhanced diffusion in polymers, which resulted in significant decreases in process time.[10] Such benefits are of importance to diffusion limited processes, such as diffusion within thermally sensitive materials or diffusion limited reactions.

CONCLUSIONS

Nonthermal microwave effects on the transport behavior of solvent and reagent in *a*-PS have been established through MD simulations using a chain of Nosé-Hoover thermostats, a high electric field intensity of 0.1 V/Å, and a range of e/m field frequencies up to 10^4 GHz. The accuracy of DCM/*a*-PS simulations has been tested against experimental NMR
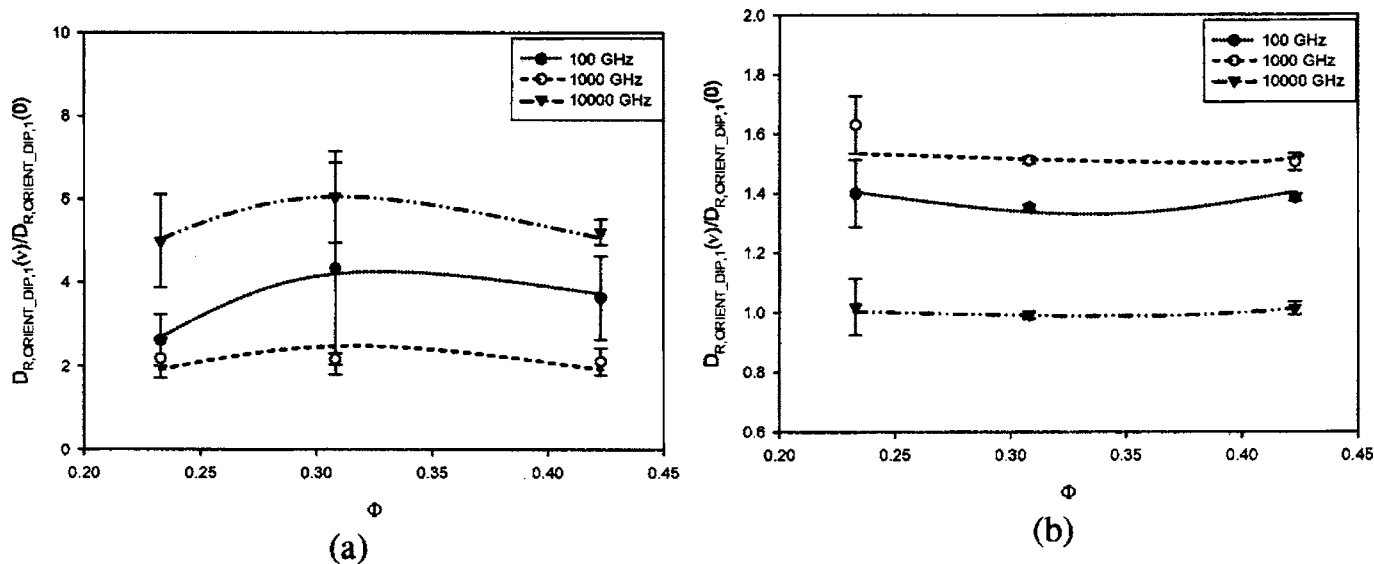

FIG. 10. Molecular dipole orientation rotational diffusion coefficient relative to zero-field conditions at 25 °C in methylamine/DCM/*a*-PS solutions over a range of frequencies and polymer densities and at a rms electric field intensity of 0.1 V/Å: (a) methylamine and (b) DCM.
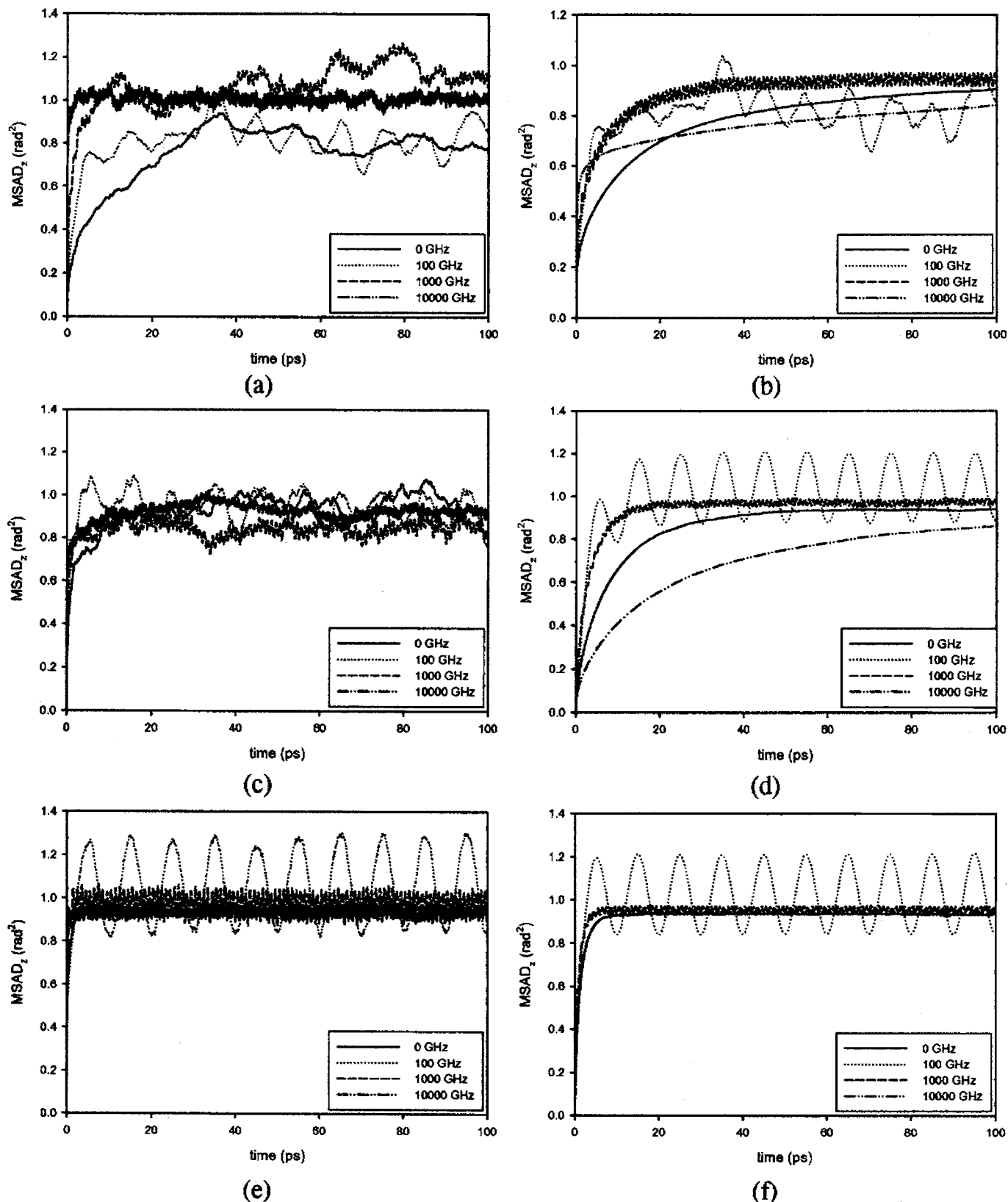
FIG. 11. The z component of the reagent and solvent mean squared angular displacement at 25 °C in methylamine/solvent/a-PS solutions (a-PS density $=0.5$ g/cm^3) over a range of frequencies and a rms electric field intensity of 0.1 V/Å: (a) Mamine in MeOH, (b) MeOH, (c) mamine in DMF, (d) DMF, (e) mamine in DCM, and (f) DCM.

diffusion measurements in the absence of an externally applied e/m field and the simulated potential models perform best at high solvent loadings. Extending the scope of simulation results to e/m field environments has been discussed

previously.[1] The method of application of the external e/m field has been tested on three solvent systems in a-PS, which included observations of the oscillation of the electric dipole moment in the direction of the electric component of the e/m

field.[21] The simulated dynamical results cover a range of e/m field frequencies up to 10^4 GHz and predict nonthermal effects in real polystyrene systems in e/m fields. Such effects are associated with coordinated molecular interactions as distinct from random molecular collisions.

Furthermore, the generated results represent local behavior that likely occurs in specific domains of real cross-linked polystyrene (which is composed of regions of differing polymer densities). The observed mobility enhancements are therefore expected to correspond to an appropriate average of the simulated results and this averaging is dependent on the macroscopic description of the polymer domains. Together with macroscopic modeling, it is hoped that MD simulations of polymer solutions in external e/m fields can ultimately quantify the likely improvements in reaction times, yields, and selectivity that may be gained using microwave technology in SPOS and offer a detailed molecular understanding of these benefits.

Experimental observations of nonthermal microwave effects in a-PS solutions at lower field strengths and frequencies might follow the same noncontact temperature measurement as in Ref. 3, noting that the distribution of reaction sites in PS beads has recently been shown by means of confocal Raman and fluorescence microscopies to be uniform.[25] The difficulty with current fiber-optic temperature measurement lies with the disentanglement of the temperature of the solvated PS bead and the bulk solvent. Recent developments in polymer temperature measurement with infrared thermography[26,27] may allow progress in microwave enhanced SPOS. The current research considered only dipolar aprotic solvents, but a further possibility for SPOS is to mix ionic liquid with an organic solvent, thereby tailoring the solvent mixture for a specific set of reactions. Differential absorption of microwaves by a liquid mixture leads to differential heating and localized thermal inhomogeneities, which cannot be duplicated by conventional heating. This may offer insights into the development of new medicinally important chemistry.[28] From the above discussion, it is expected that a diversity of microwave effects may be generated at interfaces,[29] phase boundaries,[30] and local solution inhomogeneities, where the immediate environment permits a reformation of ionic or molecular clusters which may either enhance or suppress net translational motion and thereby effect a separation of species (e.g., polar from nonpolar moieties).

[1] M. J. Purdue, J. M. D. MacElroy, D. F. O'Shea, M. O. Okuom, and F. D. Blum, J. Chem. Phys. **124**, 204904 (2006).
[2] K. Y. Tsujita, C. H. Yoshimizu, and C. M. Miyamoto, U.S. Patent No. US6706088 B2 (2004).
[3] Y. Nakai, Y. Tsujita, and H. Yoshimizu, Desalination **145**, 375 (2002).
[4] S. Gopalakrishnan, J. Münch, R. Hermann, and W. Schwieger, Chem. Eng. J. **120**, 99 (2006).
[5] S. Kataoka, D. T. Tompkins, M. A. Anderson, M. E. Zom, W. A. Zeltner, and J. H. Booske, *Proceedings of the Second World Congress on Microwave and Radio Frequency Processing*, Orlando, FL, 2–6 April 2000 (American Ceramic Society, Washington D.C., 2000).
[6] F. Al-Obeidi, R. E. Austin, J. F. Okonya, and D. R. S. Bond, Mini Reviews in Medicinal Chemistry **3**, 449 (2003).
[7] H. Tye and M. Whittaker, Org. Biomol. Chem. **2**, 813 (2004).
[8] G. C. B. Harriman, Tetrahedron Lett. **38**, 5591 (1997).
[9] J. Alcázar, J. Comb. Chem. **7**, 353 (2005).
[10] C. Gibson, I. Matthews, and A. Samuel, J. Microwave Power Electromagn. Energy **23**, 17 (1988).
[11] M. Ferrario and M. W. Evans, Chem. Phys. **72**, 141 (1982).
[12] R. W. Impey, M. Sprik, and M. L. Klein, J. Am. Chem. Soc. **109**, 5900 (1987).
[13] M. Müller, Ph.D. thesis, Swiss Federal Institute of Technology, 1999.
[14] M. Mondello, H. J. Yang, H. Furuya, and R. J. Roe, Macromolecules **27**, 3566 (1994).
[15] M. P. Allen and D. J. Tildesley, *Computer Simulation of Liquids*, 1st ed. (Clarendon, Oxford, 1987).
[16] J. Lekner, Physica A **176**, 485 (1991).
[17] B. Knopp, U. W. Suter, and A. A. Gusev, Macromolecules **30**, 6107 (1997).
[18] N. J. English and J. M. D. MacElroy, J. Chem. Phys. **118**, 1589 (2003).
[19] J. S. Vrentas and J. L. Duda, J. Polym. Sci., Polym. Phys. Ed. **15**, 403 (1977).
[20] J. S. Mackie and P. Meares, Proc. R. Soc. London, Ser. A **232**, 498 (1955).
[21] M. J. Purdue, Ph.D. thesis, University College Dublin, 2005.
[22] R. H. Perry and D. W. Green, *Perry's Chemical Engineers Handbook*, 7th ed. (McGraw-Hill, New York, 1997).
[23] G. J. Martyna, M. E. Tuckerman, and M. L. Klein, J. Chem. Phys. **97**, 2635 (1992).
[24] H. C. Anderson, J. Comput. Phys. **52**, 24 (1983).
[25] J. Kress, R. Zanaletti, A. Rose, J. G. Frey, W. S. Brocklesby, M. Ladlow, and M. Bradley, J. Comb. Chem. **5**, 28 (2003).
[26] A. Bendada, K. Cole, M. Lamontagne, and Y. Simard, J. Opt. A, Pure Appl. Opt. **5**, 464 (2003).
[27] G. M. Fike, J. Abedi, and S. Banerjee, Ind. Eng. Chem. Res. **43**, 4178 (2004).
[28] A. de la Hoz, Á. Díaz-Ortiz, and A. Moreno, Chem. Soc. Rev. **34**, 164 (2005).
[29] J. H. Booske, R. F. Cooper, and S. A. Freeman, Mater. Res. Innovations **1**, 77 (1997).
[30] A. Miklav, ChemPhysChem **2**, 552 (2001).